Bifurcation Indicator Based on Meshless and Asymptotic Numerical Methods for Nonlinear Poisson Problems

Abdeljalil Tri, Hamid Zahrouni, Michel Potier-Ferry

Bifurcation Indicator Based on Meshless and Asymptotic Numerical Methods for Nonlinear Poisson Problems

Abdeljalil Tri,[1] **Hamid Zahrouni,**[2] **Michel Potier-Ferry**[2]
[1] *Laboratoire de Mécanique, Faculté des Sciences Ain Chok Université Hassan II, Casablanca, Morocco*

[2] *Université de Lorraine, Laboratoire d'Etude des Microstructures et de Mécanique des Matériaux (LEM3), UMR CNRS 7239, Ile du Saulcy, 57045 Metz, France*

Received 2 March 2012; accepted 6 November 2013
Published online 28 January 2014 in Wiley Online Library (wileyonlinelibrary.com).
DOI 10.1002/num.21851

We propose in this work new algorithms associating asymptotic numerical method and meshless discretization (MFS-MPS: Method of fundamental solutions-Method of particular solutions) to compute branch solutions of nonlinear Poisson problems. To detect singular points on these branches, geometrical indicator, Padé approximants, and analytical bifurcation indicator are proposed. Numerical applications show the robustness and the effectiveness of the proposed algorithms. © 2014 Wiley Periodicals, Inc. Numer Methods Partial Differential Eq 30: 978–993, 2014

Keywords: asymptotic numerical method; bifurcation indicators; meshless methods; method of particular solutions; nonlinear poisson problem; padé approximants

I. INTRODUCTION

Detection of bifurcation points is a difficult challenge. The simplest technique for solving bifurcation problems is to apply a path following technique to a perturbed problem, what can now be done with the help of commercial computation codes, see for instance [1], but the difficulty of controlling the calculation increases when the perturbation gets smaller. Two main classes of algorithms are used to locate bifurcation points along a solution path without introducing perturbation. In the first class, one tries to solve the system characterizing the singular points, called extended system [2]. In the second, one computes a scalar parameter (determinant or small eigenvalue of the tangent matrix, current stiffness parameter [3]). In any case, it is not easy to establish reliable computation tools in the presence of bifurcation.

In this article, three methods will be applied to find bifurcation points, each of them being associated with asymptotic numerical method (ANM). This method consists in the association

Correspondence to: Hamid Zahrouni, Université de Lorraine, Laboratoire d'Etude des Microstructures et de Mécanique des Matériaux (LEM3), UMR CNRS 7239, Ile du Saulcy, 57045 Metz, France (e-mail: hamid.zahrouni@univ-lorraine.fr)

of Taylor series expansions and a spatial discretization method. It has been successfully applied in nonlinear solid and fluid mechanics [4–18]. An advantage of this method is an adaptive step length that is related to the convergence radius of the series. The first method to find bifurcation is based on geometrical accumulation of these steps because it has been established that the radius of convergence is strongly connected to the distance from the starting point to bifurcation point [13]. From the Taylor series, an improved representation of the solution path can be build in the form of rational fraction, called Padé approximants [19, 20]. It has been proved that the denominator of this fraction vanishes at the nearest bifurcation point. This is the second technique used in this article to detect bifurcation points [16]. The third method is to compute a scalar bifurcation indicator along the nonlinear solution branches. It is a measure of the tangent stiffness that has been introduced by Boutyour in solid mechanics [7] and by Tri in fluid mechanics [6]. A variant for Hopf bifurcation has been proposed in [9]. Several applications of these indicators have been done in solid [17, 18, 21] and fluid mechanics [6, 8, 11, 12, 15].

The originality of this work consists in associating the bifurcation indicators and a meshless technique. Here, we are particularly interested in the so called MFS-MPS (method of fundamental solutions-method of particular solutions) for the simplicity of its numerical implementation and for robustness to solve partial differential equations with variables coefficients. Meshless methods have been generally proposed to alleviate a part of the difficulties encountered in the classical finite element method (FEM) issue of domain meshing and to avoid mesh distortion [22–29]. Each meshless technique relies on the choice of a class of shape functions. Among these techniques, the MFS, first introduced by Kupradze and Aleksidze [30], has been proven to be a highly effective discretization method when the fundamental solutions of the governing equations are available [20, 22, 31]. Radial basis functions (RBF) are another class of shape functions that is very popular to solve partial differential equations since Kansa's pioneer work [32]. Recently, a numerical scheme using MFS and RBF has been proposed to further improve MFS for solving partial differential equations with variable coefficients [29, 32–36]. In this approach, the fundamental solutions and the particular solutions using RBF have been used as two classes of shape functions to approximate the partial differential equations [22, 37]. This numerical scheme will be referred as MFS-MPS. This method has the advantage of being able to solve partial differential equations with variable coefficients while generally the MFS cannot. Note that ANM is usually associated with the classical method of discretization based on the FEM. Here, we extend the application field of ANM using other discretization methods especially meshfree ones. Only the discretization technique is different between the classical ANM and the one presented in this work.

This article is dedicated to determining bifurcation points particularly on the primary branches of nonlinear Poisson problems. In Section 2, we present briefly the ANM to solve these nonlinear problems. In Section 3, we show different methods to detect bifurcation points and introduce the bifurcation indicator based on ANM. Section 4 details the meshless method, principally the MFS-MPS method, to discretize the resulting linear problems. In Section 5, we present numerical results to validate our algorithms.

II. BRANCH SOLUTIONS FOR NONLINEAR POISSON PROBLEMS

A. Problem Formulation

We consider a nonlinear Poisson problem governed by the following equation:

$$\Delta u + N(u, \lambda) = 0 \quad \text{in } \Omega \tag{1}$$

where u represents the unknown variable, λ is a loading parameter and $N(u,\lambda)$ is a nonlinear operator. The boundary conditions are:

$$u = \lambda g \text{ over } \partial\Omega \tag{2}$$

where g is given over $\partial\Omega$. It should be noted that only Dirichlet boundary conditions are considered here. However, other boundary conditions (Neumann, Robin, or mixte conditions) can be easily introduced. In this work, the nonlinear operator is chosen first in the form $N(u,\lambda) = u^2 - \lambda u$ and second in the form $N(u,\lambda) = u^2 - \lambda u - \lambda\zeta f$ to compute primary and bifurcated branches and to detect bifurcation points. The term $\lambda\zeta f$ plays the role of numerical default, ζ is a small parameter, and f is a given function. For very small values of ζ, the solution is close to the solution branch without perturbation. Note that $N(u,\lambda)$ is chosen in a quadratic form well adapted to ANM framework but more complex expression can be considered [10, 38, 39]. In the following sections, we present the main ideas of ANM and of detection of bifurcation points. To simplify the analysis, we deal with the following eigenvalue nonlinear Poisson problem:

$$\begin{cases} \Delta u + u^2 - \lambda u = 0 & \text{in } \Omega \\ u = \lambda g & \text{over } \partial\Omega \end{cases} \tag{3}$$

B. Computation of the Solution Branch by ANM

The basic idea of ANM consists in searching the solution branches of the nonlinear problem (3) in the form of a truncated Taylor expansion from a known and regular solution (u_0, λ_0),

$$(u(a), \lambda(a)) = (u_0, \lambda_0) + \sum_{i=1}^{p} a^i (u_i, \lambda_i) \tag{4}$$

where p is the truncation order of the asymptotic expansions. The control parameter $'a'$ can be defined as:

$$a = \langle u - u_0, u_1 \rangle + (\lambda - \lambda_0)\lambda_1 \tag{5}$$

with $\langle .,. \rangle$ being the Euclidian scalar product. The expansions (4) are introduced into Eqs. (3) and (5) and by equating like powers of $'a'$, we obtain a set of linear problems:

Order 1:

$$\begin{cases} L_t^0(u_1) = \lambda_1 u_0 & \text{in } \Omega \\ u_1 = \lambda_1 g & \text{over } \partial\Omega \\ \langle u_1, u_1 \rangle + \lambda_1^2 = 1 & \text{in } \Omega \end{cases} \tag{6}$$

Order k (with $2 \le k \le p$):

$$\begin{cases} L_t^0(u_k) = \lambda_k u_0 - \sum_{i=1}^{k-1} u_i u_{k-i} + \sum_{i=1}^{k-1} \lambda_i u_{k-i} & \text{in } \Omega \\ u_k = \lambda_k g & \text{over } \partial\Omega \\ \langle u_k, u_1 \rangle + \lambda_1 \lambda_k = 0 & \text{in } \Omega \end{cases} \tag{7}$$

where $L_t^0(u_j) = \Delta(u_j) + (2u_0 - \lambda_0)(u_j)$ is the tangent operator computed at the starting point (u_0, λ_0). It should be noted that the linear problems (6-7) have the same tangent operator and differ from their right-hand sides (which depend on the previous computed solutions).

The asymptotic expansions can be replaced by equivalent rational approximations, called Padé approximants [19, 20]:

$$(u(a), \lambda(a)) - (u_0, \lambda_0) = \sum_{i=1}^{p-1} \frac{PN_{p-1-i}(a)}{PD_{p-1}(a)} a^i (u_i, \lambda_i) \tag{8}$$

where PN_k and PD_k are polynomials of degree k (see Appendix for more details). This rational representation improves the validity range of the polynomial approximation but cannot obtain the whole solution branch. To do that, the path following technique is used. The validity range is determined automatically by the maximal value $a_{\max}$ of the control parameter $'a'$. Requiring that the relative difference between two consecutive orders must be smaller than a given parameter ϵ leads to [40],

$$\epsilon = \frac{\|u_p(a_{\max}) - u_{p-1}(a_{\max})\|}{\|u_p(a_{\max}) - u_0\|} \tag{9}$$

In practice, the norm $\|.\|$ in (9) is chosen as the Euclidean norm. Note that within ANM, the starting point (u_0,λ_0) of each step is known. In the applications of Section 5 and in many other cases, the starting point of the first step is (u_0, λ_0)=(0,0). In the next ones, the starting point is the end point of the previous step $(u_0 = u(a_{\max}), \lambda_0 = \lambda(a_{\max}))$ where $a_{\max}$ is computed by formulae (9). One can also insert correction phases at the beginning of some steps. Especially, ANM-corrective algorithms are available that are based on homotopy transformations [10, 41, 42]. In this manner, one defines a continuation technique allowing the determination of the whole solution branch.

III. DETECTION OF BIFURCATION POINTS

To detect bifurcation pointsin, one distinguishes three methods. The first one consists to localize the bifurcation point geometrically by exploiting an important characteristic of ANM. Indeed, it has been shown that near the bifurcation points, step accumulation appears on the branch solution [8, 13]. After this accumulation, the solution can leave the primary solution branch and follow the bifurcated one. In the other hand, the bifurcation points can be detected by analyzing a posteriori the rational representation (8). It has been early recognized that a bifurcation point corresponds to a root of the denominator [16]. The rational representation should be able to provide, first the response curve before and after the bifurcation, second the exact location of the bifurcation point. The third method to detect the bifurcation point is to define a bifurcation indicator which is well adapted to ANM. It is obtained by introducing a fictitious perturbation in the problem. By evaluating this indicator, all the critical points existing on this branch can be determined. The bifurcation point corresponds then to the zeros of this scalar indicator. In this work, we are mainly interested to this bifurcation indicator.

A. Direct Computation of the Bifurcation Indicator

In this section, we first recall how this indicator is introduced. The nonlinear problem is perturbed by a vector μf_μ where f_μ is a random function and μ is the unknown intensity of the perturbation. As consequence, the primary solution is perturbed by the fluctuation δu. Let us denote the new solution by

$$v = u + \delta u \tag{10}$$

Inserting this expression (10) into Eq. (3) and neglecting second-order terms in δu, we obtain the following new problem:

$$\begin{cases} L_t(\delta u) = \Delta\delta u + 2u\delta u - \lambda\delta u = \mu f_\mu & \text{in } \Omega \\ \delta u = 0 & \text{over } \partial\Omega \end{cases} \tag{11}$$

L_t is the tangent operator. A supplementary condition has to be imposed to obtain a well-posed problem. As for instance in the classical linearized arclength corrective algorithm, we shall seek δu in an hyperplane, which leads to the following relationship:

$$\langle \delta u - \delta u_0, \delta u_0 \rangle = 0 \tag{12}$$

In other words, the shape of the right hand side f_μ is given, its size μ is unknown, hence as a counterpart, the shape of the response δu is unknown and an additional condition about its size can be enforced. In the same spirit, instead of (12), one could prescribe the norm of δu. In case of mechanical structures, the indicator is the ratio between a force and a displacement so that it can be considered as measure of the tangent stiffness.

The initial fluctuation δu_0 is solution of the perturbed problem for $\mu = 1$:

$$L_t(\delta u_0) = f_\mu \tag{13}$$

Finally, the system to be solved is written as:

$$\begin{cases} L_t(\delta u) = \mu f_\mu & \text{in } \Omega \\ \langle \delta u - \delta u_0, \delta u_0 \rangle = 0 & \text{in } \Omega \\ \delta u = 0 & \text{over } \partial\Omega \end{cases} \tag{14}$$

The scalar μ represents the bifurcation indicator. When the operator $L_t(.)$ is singular, the indicator is equal to zero. This scalar μ and the fluctuation δu can be computed using:

$$\begin{cases} \mu = \frac{\langle \delta u_0, \delta u_0 \rangle}{\langle L_t^{-1} f_\mu, \delta u_0 \rangle} & \text{in } \Omega \\ \delta u = \mu L_t^{-1} f_\mu & \text{in } \Omega \\ \delta u = 0 & \text{over } \partial\Omega \end{cases} \tag{15}$$

The first equation of (15) gives the scalar μ for each value of λ and called "the direct computation" of the indicator. This method is very expensive in computing time for the higher number of unknowns. To avoid this restriction, we use the ANM by expanding the unknowns $(\delta u, \mu)$ into polynomial approximations with respect to the path parameter $'a'$.

B. Computation of the Bifurcation Indicator by ANM

The fluctuation and the indicator are searched in the form of a truncated Taylor expansion from a known solution $(\delta u_0, 1)$,

$$(\delta u(a), \mu(a)) = (\delta u_0, 1) + \sum_{i=1}^{p} a^i (\delta u_i, \mu_i) \tag{16}$$

These expansions (16) are introduced into Eq. (14) to obtain the linear problems at each order k ($1 \leq k \leq p$):

$$\begin{cases} L_t^0(\delta u_k) = \mu_k f_\mu - \sum_{i=1}^{k} 2u_i \delta u_{k-i} + \sum_{i=1}^{k} \lambda_i \delta u_{k-i} & \text{in } \Omega \\ \delta u_k = 0 & \text{over } \partial\Omega \\ \langle \delta u_k, \delta u_0 \rangle = 0 & \text{in } \Omega \end{cases} \tag{17}$$

where L_t^0 is exactly the same tangent operator defined in Eqs. (6) and (7). The bifurcation indicator is computed after determining the primary branch solution by computing all the terms (u_k, λ_k). The asymptotic expansions (16) can be also replaced by Padé approximants:

$$(\delta u(a), \mu(a)) - (\delta u_0, 1) = \sum_{i=1}^{p-1} \frac{PN_{p-1-i}(a)}{PD_{p-1}(a)} a^i (\delta u_i, \mu_i) \tag{18}$$

The bifurcation point can be then detected by the zeros of the indicator given by Eqs. (16) or (18).

IV. SPATIAL DISCRETIZATION USING THE MFS-MPS METHOD

In this section, we propose to solve the linear problems (6-7 and 17) by using MFS-MPS method. These problems can be set in a generic form as follows:

$$\begin{cases} \Delta u + \gamma(x, y)u = f(x, y) & \text{in } \Omega \\ u = g(x, y) & \text{over } \partial\Omega \end{cases} \tag{19}$$

Since the general differential operators have nonconstant coefficients, the fundamental solution is not available. This boundary value problem can be converted into a standard Poisson-type equation using the analog equation method [25, 26]. In this purpose, the Laplacian is kept on the left hand side and all the other terms are moved to the right hand side and are treated as forcing terms. In this way, Eq. (19) is rearranged into Poisson's equation:

$$\begin{cases} \Delta u = -\gamma(x, y)u + f(x, y) = h(x, y, u) & \text{in } \Omega \\ u = g(x, y) & \text{over } \partial\Omega \end{cases} \tag{20}$$

which can be easily solved by the well-known MFS-MPS method. Here, we briefly introduce the technique of the newly developed MFS-MPS. This method is based on the idea that the solution can be written as the sum of a particular solution and the general solution of the homogeneous equation. Hence, we assume that the approximate solution of (20) can be written in the following form:

$$u(x, y) = \sum_{i=1}^{N_t} \alpha_i v(r_i) + \sum_{j=1}^{N_b} \beta_j G(\rho_j) \tag{21}$$

where N_t and N_b represent, respectively, the number of points in Ω and the number of points over $\partial\Omega$. $v(r)$ represents a particular solution of the Laplace operator defined by

$$\Delta v(r) = \phi(r) \tag{22}$$

The known function ϕ combines RBF which approximate the right hand side of (20-a) as follows

$$h(x, y, u) = \sum_{i=1}^{N_t} \alpha_i \phi(r_i) \tag{23}$$

where $r_i = \|(x, y) - (x_i, y_i)\|, (x_i, y_i)_{i=1..N_t}$ are called trial points in the domain Ω. Note that $\{\alpha_i\}_{i=1}^{N_t}$ are the unknown coefficients to be determined. Note also that

$$G(\rho) = -\frac{1}{2\pi} \log(\rho) \tag{24}$$

is the fundamental solution of the Laplace operator for 2D problem characterized by

$$\Delta G(\rho) = 0 \tag{25}$$

where $\rho_i = \|(x, y) - (xs_i, ys_i)\|, (xs_i, ys_i)_{i=1..N_b}$ are the source points that are be chosen on a curve Γ outside the domain that is called fictitious or virtual boundary. Within the classical versions of MFS [22, 23], the two terms of (21) can be computed separately: the particular solution permits to balance the right hand side of the Eq. (20-a) and next the fundamental solutions are defined in such way that they balance the boundary data. This splitting into an interior problem and a boundary only problem cannot be done here because the fundamental solutions do not belong to the kernel of the tangent operator (6), (7), or (17). Instead of finding the particular solution and homogeneous solution separately, we intend to obtain the undetermined coefficients $\{\alpha_i\}_{i=1}^{N_t}$ and $\{\beta_i\}_{i=1}^{N_b}$ simultaneously. Using RBF approximation (23) and introducing (21) into (20), we obtain,

$$\sum_{i=1}^{N_t} \alpha_i \Psi(r_i) + \sum_{j=1}^{N_b} \beta_j \Theta(\rho_j) = f(x, y) \quad (x, y) \in \Omega \tag{26}$$

where

$$\Psi(r_i) = \Delta v(r_i) + \gamma(x, y) v(r_i) = \phi(r_i) + \gamma(x, y) v(r_i) \tag{27}$$

and

$$\Theta(\rho_i) = \Delta G(\rho_i) + \gamma(x, y) G(\rho_i) = \gamma(x, y) G(\rho_i) \tag{28}$$

The boundary condition (20-b) becomes

$$\sum_{i=1}^{N_t} \alpha_i v(r_i) + \sum_{j=1}^{N_b} \beta_j G(\rho_j) = g(x, y) \quad (x, y) \in \partial\Omega \tag{29}$$

$\Psi(r)$ and $\Theta(\rho)$ are known functions. For the implementation, one chooses N_t interior points in Ω and N_b boundary points over $\partial\Omega$ and the same source points on the fictitious boundary Γ. By collocation, Eqs. (26) and (29) lead to the following $(N_t + N_b) \times (N_t + N_b)$ system of equations:

$$\begin{bmatrix} \Psi(r_{ij}) & \Theta(\rho_{ij}) \\ v(r_{ij}) & G(\rho_{ij}) \end{bmatrix} \begin{Bmatrix} \alpha \\ \beta \end{Bmatrix} = \begin{Bmatrix} f \\ g \end{Bmatrix} \tag{30}$$

Once the coefficients $\{\alpha_i\}_{i=1}^{N_t}$ and $\{\beta_i\}_{i=1}^{N_b}$ are determined by solving (30), the approximate solution u can be obtained from (21). Effectiveness and accuracy of the interpolation depend on the choice of the approximating functions ϕ. Global interpolation functions, such as Lagrange polynomials, Fourier sine and cosine series, RBFs of polynomial type, thin plate spline and multiquadric (MQ) functions may be used for this purpose [23–26, 29, 32, 33]. In this article, the functions ϕ in Eq. (23) are selected to be MQ RBFs with respect to a Euclidian distance r,

$$\phi(r) = \sqrt{c^2 + r^2} \tag{31}$$

where c is a given parameter. Next the use of Eqs. (22) and (31) give the approximating particular solutions $v(r)$ by

$$v(r) = \frac{1}{9}(4c^2 + r^2)\sqrt{c^2 + r^2} - \frac{c^3}{3}\log(c + \sqrt{c^2 + r^2}) \tag{32}$$

for two-dimensional (2D) problems.

V. NUMERICAL APPLICATIONS

The proposed method has been applied to several examples. Here, we limit ourselves to two main tests which present bifurcation points and nonlinear solution branches. The first problem concerns a nonlinear eigenvalue problem on square domain where the bifurcation points and the eigenmodes are known analytically. The second is a nonlinear Poisson problem in a circular domain. For the solution branch within ANM, two main parameters are important: the truncation order and the parameter ϵ of Eq. (9). It has been shown in previous papers that the optimum truncation order is generally in the range $15 - 30$ [5–11, 40]. The parameter ϵ defines the step length in the continuation technique. The resulting linear problems are discretized by MFS-MPS method with the use of MQ radial basis functions. The constant c is chosen equal to 1.5. This choice is based primarily on the work of Golberg et al. [23] which used a cross validation algorithm to obtain the optimal value of the parameter c. It is important to note that we have used different values of c and also other basic functions particularly polynomial functions and we have obtained the same results.

Example 1. We consider the nonlinear Poisson problem in a square domain (Fig. 1):

$$\begin{cases} \Delta u + u^2 - \lambda u = \lambda \xi f & \text{in } \Omega \\ u = 0 & \text{over } \partial\Omega \end{cases} \tag{33}$$

where $\Omega = [0, 1] \times [0, 1]$. In this example, nine points were chosen inside the square and 16 points on the boundary $\partial\Omega$ and the same number of source points are uniformly distributed on the fictitious boundary square $[-4, 5] \times [-4, 5]$.

For this example, the bifurcation points λ_b and the eigenmodes u_b are known analytically:

$$\begin{cases} \lambda_b = (m^2 + n^2)\pi^2 \\ u_b = \sin(m\pi x)\sin(n\pi y) \end{cases} \tag{34}$$

where m and n are integer numbers. Here, we are interested in the first bifurcation which is given for $m = 1$ and $n = 1$. The right hand side term $\lambda\xi f$ of (33) plays the role of numerical default and

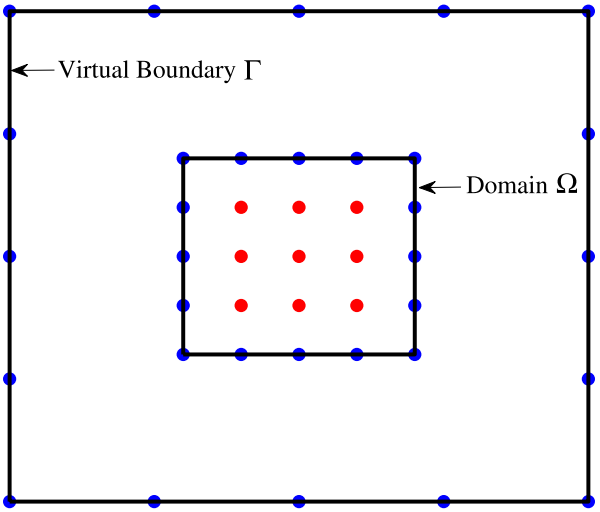

FIG. 1. Discretization of the square domain and the fictitious boundary Γ. [Color figure can be viewed in the online issue, which is available at wileyonlinelibrary.com.]

allows automatically following bifurcated branches. A similar behavior is observed in buckling problems when a default is introduced [7, 16]. To be very close the bifurcation point, the parameter ξ must be very small and it is taken here equal to $\pm 10^{-6}$. To illustrate this idea, the variable u measured at the location $(x = 0.5, y = 0.5)$ is plotted versus the parameter λ in Fig. 2. In this figure, step accumulation is observed for λ close to 19.75 (each step in the continuation procedure is represented by a circle symbol for $\xi = -10^{-6}$ and square symbol for $\xi = 10^{-6}$ on the curves). After this step accumulation, the numerical solution switches to a bifurcated branch instead of staying on the primary solution which indicates geometrically the first bifurcation point. We then apply the procedure to detect the bifurcation point using the different methods previously presented. Figure 3 shows the evolution of the indicator versus the parameter λ using the polynomial

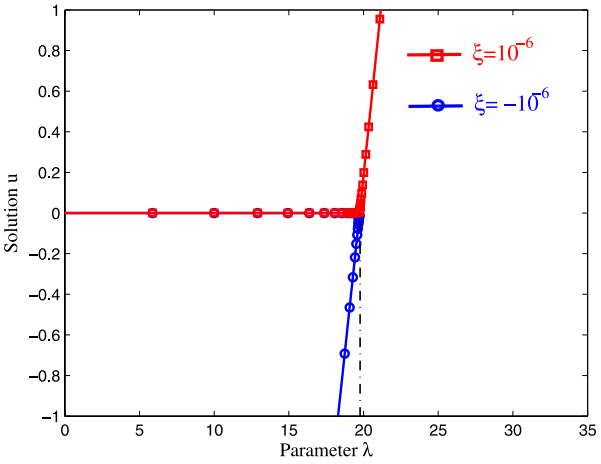

FIG. 2. Solution branches by ANM-MFS-MPS for $\xi = 10^{-6}$ and $\xi = -10^{-6}$. [Color figure can be viewed in the online issue, which is available at wileyonlinelibrary.com.]

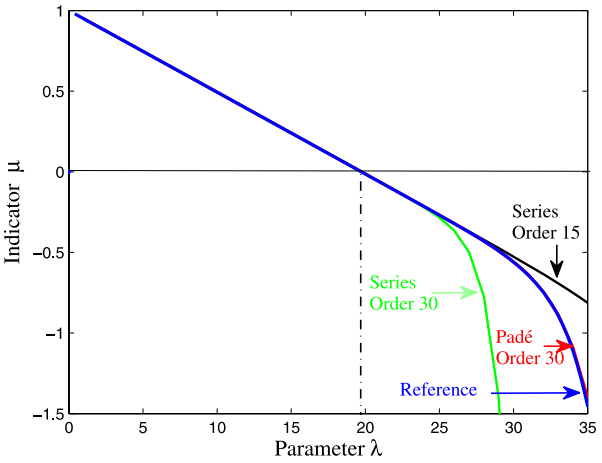

FIG. 3. Indicator μ versus λ by ANM-MFS-MPS for different truncation orders of the series (16), Padé approximants (18) and by formulae (15). [Color figure can be viewed in the online issue, which is available at wileyonlinelibrary.com.]

expansion (16) with the two truncation orders 15 and 30, Padé approximants (18) with order 30 and the direct computation given by the formula (15) which is considered as the reference curve. These indicators are null for $\lambda = 19.75$. The same value of the first bifurcation has been recovered from the first real root of the denominator of the Padé approximants, see Eq. (8). These estimates of the critical point coincide with the exact analytical value. To reach the bifurcation point by ANM, one needs only one step, that is one triangulation of the tangent matrix. In other words, the geometrical indicator (accumulation of steps), the indicator based on the Taylor series (16) and the pole of the Padé approximants (8) give the same result as the analytical solution. This result confirms the effectiveness of our algorithms in computing bifurcation points. Note also that it is very difficult to compute a bifurcation branch with a so small imperfection by using a classical incremental-iterative method: the adaptive step length of ANM has permitted to perform this calculation with high truncation order $p = 15$ and with an accuracy parameter $\epsilon = 10^{-6}$.

Finally, we discuss shortly the accuracy of the method with respect to the discretization technique and the truncation order of the series. To investigate the influence of the number of collocation points and the truncation order of the series, we calculate the relative errors $\kappa = |\frac{\lambda - \lambda_b}{\lambda_b}|$ between the numerical solution λ at the bifurcation point and the analytical solution λ_b. The results are presented in Table I. It is observed that the numerical solution is insensitive to the truncation order: the choice of a very small ϵ ensures a quasiexact solving of the discrete nonlinear system so that the error is only due to the discretization. We display in the same table the results of the error κ for several numbers of collocation points in the domain. The results become more and more accurate by increasing the number of points and a very high accuracy is obtained (κ close 10^{-5} from 25 points). Next one reaches a plateau and a slight decrease, what is common within meshless methods and can be due to matrix ill-conditioning [43].

Example 2. We consider the following nonlinear Poisson problem in a circle domain:

$$\begin{cases} \Delta u + u^2 = \lambda f & \text{in } \Omega \\ u = \lambda g & \text{over } \partial\Omega \end{cases} \tag{35}$$

TABLE I. Comparison of ANM-MFS-MPS solution and the analytical one at the bifurcation point for different number of points in the domain and for different truncation orders.

		Order 5	Order 10	Order 15	Order 20	Order 30
9 points	λ	20.2605	20.2605	20.2605	20.2606	20.2604
	κ	2.6410E-2	2.6409E-2	2.6409E-2	2.6414E-2	2.6407E-2
16 points	λ	19.8199	19.8199	19.8199	19.8199	19.8199
	κ	4.0900E-3	4.0895E-3	4.0888E-3	4.0881E-3	4.0891E-3
25 points	λ	19.7389	19.7387	19.7386	19.7385	19.7383
	κ	1.1966E-5	2.5718E-5	3.0784E-5	3.4250E-5	4.1593E-5
36 points	λ	19.7389	19.7388	19.7388	19.7383	19.7386
	κ	1.1966E-5	1.5990E-5	1.8629E-5	1.3725E-5	2.8104E-5
42 points	λ	19.7333	19.7410	19.7275	19.7302	19.7276
	κ	2.9720E-4	9.5565E-5	5.8953E-4	4.5500E-4	5.8431E-4

where $\Omega = x^2 + y^2 - 1 \leq 0$, $g = x^2 + y^2$, and $f = 4 + (x^2 + y^2)^2$. The geometrical description of this example is shown in Fig. 4. In fact, 69 points were chosen inside the circle and 10 points on the boundary $\partial\Omega$ and the same number of source points are uniformly distributed on the fictitious circle of radius $R = 8$ and centred at the origin. The accuracy against the fictitious boundary R and the convergence study against the number of collocation points has been already presented and discussed in this previous work [35]. In Fig. 5, the nonlinear solutions of (35) are computed with ANM-MFS-MPS and are plotted with respect to the truncation order $N = 20$ and the parameter $\epsilon = 10^{-8}$. These plots correspond to the variable u at the point $(x = -0.4286, y = 0.6429)$ versus the parameter λ. Once more, one observes step accumulation for λ close to 2.8899 which permits to localize geometrically the bifurcation point. In Figure 6, the denominator of Padé approximants of Eq. (8) is plotted versus the parameter λ along the first step. This denominator is equal to zero around $\lambda = 2.8899$ confirming the presence of the bifurcation point. Note that, we are only interested to the first real root of this denominator. The same root $\lambda = 2.8899$ is also obtained with various truncature orders, results are given in Table II. As previously, we have also

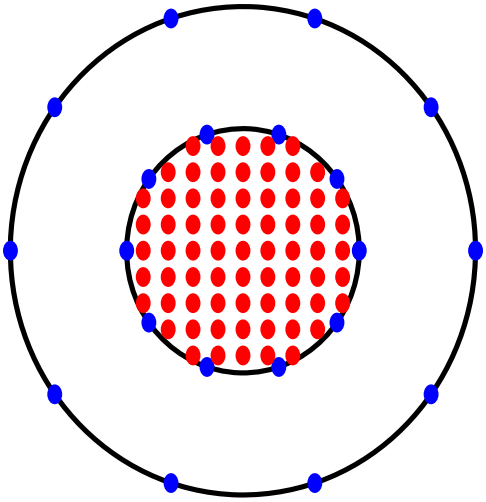

FIG. 4. Discretization of the domain, the boundary and the fictitious circle. [Color figure can be viewed in the online issue, which is available at wileyonlinelibrary.com.]

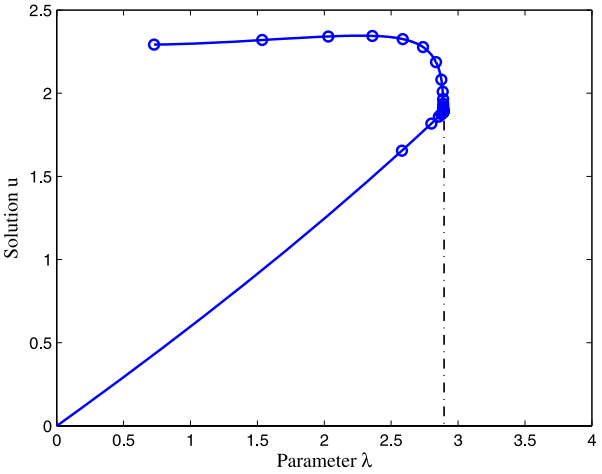

FIG. 5. Solution branch by the ANM-MFS-MPS using Taylor series (4) with $N = 20$ and $\epsilon = 10^{-8}$. [Color figure can be viewed in the online issue, which is available at wileyonlinelibrary.com.]

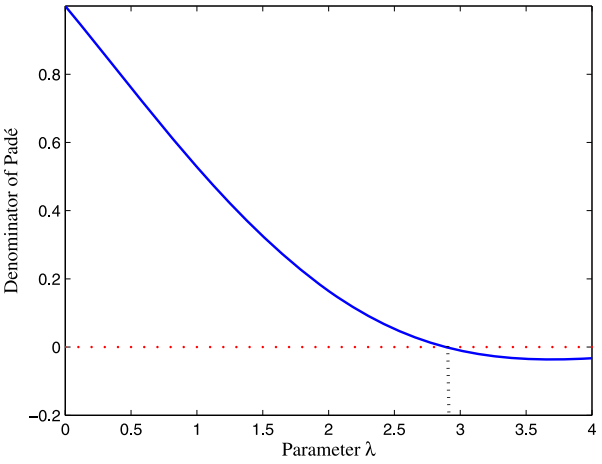

FIG. 6. Denominator of Padé approximants versus parameter λ. Bifurcation point corresponds to the first real root ($\lambda = 2.8899$) of Padé denominator. [Color figure can be viewed in the online issue, which is available at wileyonlinelibrary.com.]

computed the bifurcation indicator by the series (16) and Padé approximants (18). The result is plotted in the Fig. 7. We see that this indicator vanishes close to the same value $\lambda = 2.8899$. We conclude that the three methods permit to detect the first bifurcation point and show the robustness of our algorithms.

TABLE II. The ANM-MFS-MPS solution of the bifurcation point for different orders.

	Order 5	Order 10	Order 15	Order 20	Order 30
λ	2.8910	2.8899	2.8899	2.8899	2.8897

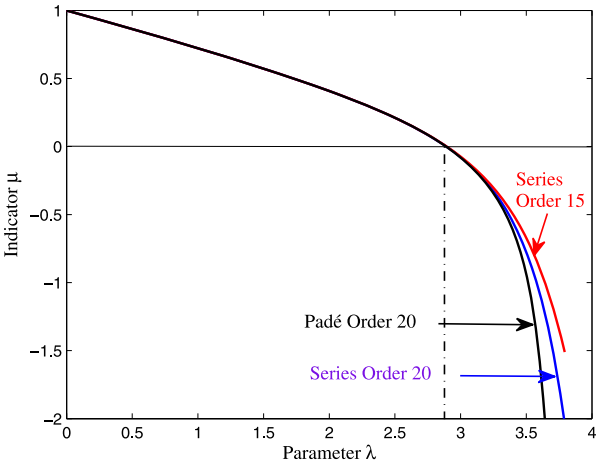

FIG. 7. Indicator μ versus λ by ANM-MFS-MPS for different truncation orders of the series (16) and Padé approximants (18). [Color figure can be viewed in the online issue, which is available at wileyonlinelibrary.com.]

VI. CONCLUSIONS

In this work, we have presented new numerical techniques combining ANM and meshless method (MFS-MPS) to compute branch solutions of nonlinear Poisson problem and to detect singular points. Three numerical techniques have been proposed for detecting singular points: i) geometrical indicator consisting in localizing step accumulation on the branch solution, ii) search of the first real root of the denominator of Padé approximants which corresponds to the first bifurcation point, iii) introduction of a bifurcation indicator which is null at bifurcation points; this indicator is developed within three procedures: direct computation (15), Taylor series (16), and Padé approximants (18). Effectiveness of the proposed algorithms has been presented for two main examples. The use of ANM allows one to obtain nonlinear solution with large and adaptive step length. Let us recall that this technique solves the nonlinear Poisson problem with high-order predictor and without need of any iteration. In the presence of bifurcation points, this technique reduces automatically the step length leading to accumulation steps. For the space discretization, we have proposed the use of the meshless method to compute the linear problems resulting from the perturbation technique. Because the linear operators have variable coefficients, the MFS-MPS method is used.

APPENDIX: PADÉ APPROXIMANTS FOR VECTORIAL SERIES

We present in this section the procedure used to compute Padé approximants in the framwork of ANM.

i. From vectors $U_1, U_2, \ldots, U_p$, we construct an orthogonal basis by using the classical Gram–Schmidt procedure (we give details for $p = 6$):

$$\begin{cases} \mathbf{U}_1 = \alpha_{11}\ \mathbf{U}_1^* \\ \mathbf{U}_2 = \alpha_{21}\ \mathbf{U}_1^* + \alpha_{22}\ \mathbf{U}_2^* \\ \mathbf{U}_3 = \alpha_{31}\ \mathbf{U}_1^* + \alpha_{32}\ \mathbf{U}_2^* + \alpha_{33}\ \mathbf{U}_3^* \\ \mathbf{U}_4 = \alpha_{41}\ \mathbf{U}_1^* + \alpha_{42}\ \mathbf{U}_2^* + \alpha_{43}\ \mathbf{U}_3^* + \alpha_{44}\ \mathbf{U}_4^* \\ \mathbf{U}_5 = \alpha_{51}\ \mathbf{U}_1^* + \alpha_{52}\ \mathbf{U}_2^* + \alpha_{53}\ \mathbf{U}_3^* + \alpha_{54}\ \mathbf{U}_4^* + \alpha_{55}\ \mathbf{U}_5^* \\ \mathbf{U}_6 = \alpha_{61}\ \mathbf{U}_1^* + \alpha_{62}\ \mathbf{U}_2^* + \alpha_{63}\ \mathbf{U}_3^* + \alpha_{64}\ \mathbf{U}_4^* + \alpha_{65}\ \mathbf{U}_5^* + \alpha_{66}\ \mathbf{U}_6^* \end{cases} \tag{A1}$$

After that, these relations are introduced in the polynomial representation leading to six polynomials with decreasing degree (from 5 to 0) with respect to vectors U_k:

$$\begin{aligned} \mathbf{U} - \mathbf{U}_0 = a\ \mathbf{U}_1^* \left(\alpha_{11} + a\alpha_{21} + a^2\alpha_{31} + a^3\alpha_{41} + a^4\alpha_{51} + a^5\alpha_{61}\right) + a^2\ \mathbf{U}_2^* \left(\alpha_{22} + a\alpha_{32}\right. \\ \left. + a^2\alpha_{42} + a^3\alpha_{52} + a^4\alpha_{62}\right) + a^3\ \mathbf{U}_3^* \left(\alpha_{33} + a\alpha_{43} + a^2\alpha_{53} + a^3\alpha_{63}\right) + \\ a^4\ \mathbf{U}_4^* \left(\alpha_{44} + a\alpha_{54} + a^2\alpha_{64}\right) + a^5\ \mathbf{U}_5^* \left(\alpha_{55} + a\alpha_{65}\right) + a^6\ \mathbf{U}_6^* \left(\alpha_{66}\right)\ . \end{aligned} \tag{A2}$$

ii. We replace the polynomials by Padé appriximants having the same denominator ($D_5 = d_1 + ad_2 + \cdots + a^5 d^5$), in the following way:

$$\begin{cases} \alpha_{11} + a\alpha_{21} + a^2\alpha_{31} + a^3\alpha_{41} + a^4\alpha_{51} + a^5\alpha_{61} \approx \frac{b_0 + ab_1 + a^2 b_2 + a^3 b_3 + a^4 b_4}{D_5} \\ \alpha_{22} + a\alpha_{32} + a^2\alpha_{42} + a^3\alpha_{52} + a^4\alpha_{62} \approx \frac{c_0 + ac_1 + a^2 c_2 + a^3 c_3}{D_5} \\ \alpha_{33} + a\alpha_{43} + a^2\alpha_{53} + a^3\alpha_{63} \approx \frac{e_0 + ae_1 + a^2 e_2}{D_5} \\ \alpha_{44} + a\alpha_{54} + a^2\alpha_{64} \approx \frac{f_0 + af_1}{D_5} \\ \alpha_{55} + a\alpha_{65} \approx \frac{g_0 + af_1}{D_5} \end{cases} \tag{A3}$$

Coefficients b_i, c_i, e_i, f_i and g_i are computed by using the same procedure as for the classical Padé approximants; by requiring that each fraction has the same Taylor expansions as the corresponding polynomials up to orders 5, 4, 3, 2, 1, respectively. This results:

$$\begin{aligned} &b_0 = \alpha_{11}\ , \\ &b_1 = \alpha_{21} + \alpha_{11}\ d_1\ , \\ &b_2 = \alpha_{31} + \alpha_{21}\ d_1 + \alpha_{11}\ d_2\ , \\ &b_3 = \alpha_{41} + \alpha_{31}\ d_1 + \alpha_{21}\ d_2 + \alpha_{11}\ d_3\ , \\ &b_4 = \alpha_{51} + \alpha_{41}\ d_1 + \alpha_{31}\ d_2 + \alpha_{21}\ d_3 + \alpha_{11}\ d_4\ , \\ &c_0 = \alpha_{22}\ , \qquad\qquad e_1 = \alpha_{43} + \alpha_{33}\ d_1\ , \\ &c_1 = \alpha_{32} + \alpha_{22}\ d_1\ , \qquad\qquad e_2 = \alpha_{53} + \alpha_{43}\ d_1 + \alpha_{33}\ d_2\ , \\ &c_2 = \alpha_{42} + \alpha_{32}\ d_1 + \alpha_{22}\ d_2\ , \qquad\quad f_0 = \alpha_{44}\ , \\ &c_3 = \alpha_{52} + \alpha_{42}\ d_1 + \alpha_{32}\ d_2 + \alpha_{22}\ d_3\ , \quad f_1 = \alpha_{54} + \alpha_{44}\ d_1\ , \\ &e_0 = \alpha_{33}\ , \qquad\qquad g_0 = \alpha_{55}\ . \end{aligned}$$

iii. After some rearrangements, we obtain a new expression of the previous rational representation involving only vectors $\mathbf{U}_k$ and coefficients d_i:

$$\mathbf{U} - \mathbf{U}_0 = a\ \frac{D_4}{D_5}\ \mathbf{U}_1 + a^2\ \frac{D_2}{D_5}\ \mathbf{U}_2 + a^3\ \frac{D_2}{D_5}\ \mathbf{U}_3 + a^4\ \frac{D_1}{D_5}\ \mathbf{U}_4 + a^5\ \frac{1}{D_5}\ \mathbf{U}_5\ . \tag{A4}$$

We use the same procedure for the parameter λ:

$$\lambda - \lambda_0 = a\ \frac{D_4}{D_5}\ \lambda_1 + a^2\ \frac{D_2}{D_5}\ \lambda_2 + a^3\ \frac{D_2}{D_5}\ \lambda_3 + a^4\ \frac{D_1}{D_5}\ \lambda_4 + a^5\ \frac{1}{D_5}\ \lambda_5\ . \tag{A5}$$

References

1. J. G. Teng and C. Y. Song, Numerical models for nonlinear analysis of elastic shells with eigenmode-affine imperfections, Int J Solids Struct 38 (2001), 3263–3280.
2. R. Seydel, Numerical computation of branch points in nonlinear equations, Numer Math 33 (1979), 339–352.
3. N. Nayar and J. M. Ortega, Computation of selected eigenvalues of generalized eigenvalue problems, J Comput Phys 108 (1993), 8–14.
4. N. Damil and M. Potier-Ferry, A new method to computed bifurcations: application to the buckling of imperfect elastic structures, Int J Eng Sci 28 (1990), 934–957.
5. A. Tri, H. Zahrouni, and M. Potier-Ferry, Perturbation technique and method of fundamental solution to solve nonlinear Poisson problems, Eng Anal Bound Elem 35 (2011), 273–278.
6. A. Tri, B. Cochelin, and M. Potier-Ferry, Résolution des équations de Navier Stokes et détection des bifurcations stationnaires par une méthode asymptotique numérique, Revue européenne des éléments finis 5 (1996), 415–442.
7. E. H. Boutyour, Méthode asymptotique numérique pour le calcul de bifurcations: application aux structures élastiques, Thesis, Université de Metz, France, 1994.
8. A. Tri, Méthode asymptotique numérique pour les fluides visqueux incompressibles et la détection de la bifurcation de Hopf, Thesis, Université de Metz, France, 1996.
9. M. E. H. Bensaadi, Méthode asymptotique numérique pour le calcul de bifurcations de Hopf et de solutions périodiques, Thesis, Université de Metz, France, 1995.
10. B. Cochelin, N. Damil, and M. Potier-Ferry, Méthode asymptotique numériques, Hermès-Lavoisier, Paris, 2007.
11. J. M. Cadou, M. Potier-Ferry, and B. Cochelin, A numerical method for the computation of bifurcation points in fluid mechanics, Eur J Mech B Fluids 25 (2006), 234–254.
12. Y. Guevel, E. H. Boutyour, and J. M. Cadou, Automatic detection and branch switching methods for steady bifurcation in fluid mechanics, J Comput Phys 230 (2011), 3614–3629.
13. S. Baguet and B. Cochelin, On the behaviour of the ANM continuation in the presence of bifurcations, Commun Numer Methods Eng 19 (2003), 459–471.
14. E. H. Boutyour, H. Zahrouni, M. Potier-Ferry, and M. Boudi, Asymptotic-numerical method for buckling analysis of shell structures with large rotations, J Comput Appl Math 168 (2004), 77–85.
15. A. Brezillon, G. Girault, and J. M. Cadou, A numerical algorithm coupling a bifurcating indicator and a direct method for the computation of Hopf bifurcation points in fluid mechanics, Comput Fluids 39 (2010), 1226–1240.
16. E. H. Boutyour, H. Zahrouni, M. Potier-Ferry, and M. Boudi, Bifurcation points and bifurcated branches by an asymptotic numerical method and padé approximants, Int J Numer Methods Eng 60 (2004), 1987–2012.
17. M. Jamal, H. Elasmar, B. Braikat, E. H. Boutyour, B. Cochelin, N. Damil, and M. Potier-ferry, Bifurcation indicators, Acta Mech 139 (2000), 129–142.
18. P. Vannucci, B. Cochelin, N. Damil, and M. Potier-Ferry, An asymptotic numerical method to compute bifurcating branches, Int J Numer Methods Eng 41 (1998), 1365–1389.
19. G. A. Baker and P. Graves-Morris, Padé approximants, Part I: basic theory, Encyclopedia of mathematics and its applications, Addison-Wesley, London, 1981.
20. A. Najah, B. Cochelin, N. Damil, and M. Potier-Ferry, A critical review of asymptotic numerical methods, Arch Comput Methods Eng 5 (1998), 3–22.
21. K. Dossou, Résolution numérique des équations de von karman, Thesis, Université Laval, Québec, 1999.
22. M. A. Golberg, The method of fundamental solutions for Poisson's equation, Eng Anal Bound Elem 16 (1995), 205–213.

23. M. A. Golberg, C. S. Chen, and S. R. Karur, Improve multiquadric interpolation for partial differential equations, Eng Anal Bound Elem 18 (1996), 9–17.

24. P. A. Ramachandran and K. Balakrishnan, Radial basis functions as approximate particular solutions: review of recent progress, Eng Anal Bound Elem 24 (2000), 575–582.

25. J. T. Katsikadelis, The analog equation method, a boundary-only integral equation for non-linear static and dynamic problems in general bodies, Theor Appl Mech 27 (2002), 13–38.

26. H. Wang and Q. H. Qin, A meshless method for generalized linear or nonlinear Poisson-type problems, Eng Anal Bound Elem 30 (2006), 515–521.

27. Z. Fu, W. Chen, and Q. Qin, Boundary knot method for heat conduction in nonlinear functionally graded material, Eng Anal Boundary Elem 35 (2011), 729–734.

28. Y. Gu, W. Chen, and C.-Z. Zhang, Singular boundary method for solving plane strain elastostatic problems, Int J Solids Struct 48 (2011), 2549–2556.

29. C. J. S. Alves and S. Valtchev, A Kansa type method using fundamental solutions applied to elliptic PDEs, V. M. A. Leitao, editor, Advances in meshfree techniques, Springer, Netherland, 2007, pp. 241–256.

30. V. D. Kupradze and M. A. Aleksidze, The method of functional equations for the approximate solution of certain boundary value problems, Comput Math Math Phys 4 (1964), 82–126.

31. J. Lin, W. Chen, and F.-Z. Wang, A new investigation into regularization techniques for the method of fundamental solutions, Math Comput Simul 81 (2011), 1144–1152.

32. E. J. Kansa, Multiquadrics a scattered data approximation scheme with applications to computational fluid dynamics.i. surface approximations and partial derivative estimates, Comput Math Appl 19 (1990), 127–145.

33. C. S. Chen, C. M. Fan, and J. Monroe, The method of fundamental solutions for solving elliptic pdes with variable coefficients, C. S. Chen, A. Karageorghis, and Y. S. Smyrlis, editors, The method of fundamental solutions - a meshless method, Dynamic Publishers, Atlanta, 2008, pp. 75–105.

34. X. Li and J. Zhu, The method of fundamental solutions for nonlinear elliptic problems, Eng Anal Bound Elem 33 (2009), 322–329.

35. A. Tri, H. Zahrouni, and M. Potier-Ferry, High order continuation algorithm and meshless procedures to solve nonlinear Poisson problems, Eng Anal Bound Elem 36 (2012), 1705–1714.

36. G. Yao, C. H. Tsai, and W. Chen, The comparison of three meshless methods using radial basis functions for solving fourth-order partial differential equations, Eng Anal Bound Elem 34 (2010), 625–631.

37. W. Chen, J. Lin, and F.-Z. Wang, Regularized meshless method for nonhomogeneous problems, Eng Anal Bound Elem 35 (2011), 253–257.

38. W. Aggoune, H. Zahrouni, and M. Potier-Ferry, Asymptotic numerical methods for unilateral contact, Int J Numer Methods Engineering 68 (2006), 605–631.

39. S. Nezamabadi, H. Zahrouni, and J. Yvonnet, Solving hyperelastic material problems by asymptotic numerical method, Comput Mech 47 (2011), 77–92.

40. B. Cochelin, A path-following technique via an asymptotic-numerical method, Comput Struct 53 (1994), 1181–1192.

41. W. Aggoune, H. Zahrouni, and M. Potier-Ferry, High-order prediction-correction algorithms for unilateral contact problems, J Comput Appl Math 168 (2004), 1–9.

42. H. Lahman, J.-M. Cadou, H. Zahrouni, N. Damil, and M. Potier-Ferry, High-order predictor-corrector algorithms, Int J Numer Methods Eng 55 (2002), 685–704.

43. E. J. Kansa and Y. C. Hon, Circumventing the ill-conditioning problem with multiquadric radial basis functions: applications to elliptic partial differential equations, Comput Math Appl 39 (2000), 123–137.